Extension of Farrenkopf Steady-State Solutions with Estimated Angular Rate

Andrew D. Dianetti* and John L. Crassidis†

University at Buffalo, State University of New York, Amherst, NY 14260-4400

Steady-state solutions of the single-axis attitude estimation filter are considered for the traditional case of dynamic model replacement, where the angular rate is determined directly from a gyroscope reading and bias estimate, and for the augmented case where the angular rate is estimated in the filter. The impact of the process noise on the steady-state values is analyzed, and it is found that there exists a value for the process noise below which the augmented filter performs better, and above which the dynamic model replacement filter performs better. A Multiple-Model Adaptive Estimation filter is developed to allow for uncertainties in assumed process noise in the augmented filter to be handled. Three-axis results are compared to single-axis results and are found to perform similarly.

Introduction

Farrenkopf developed analytic steady-state solutions for the covariance of two single-axis spacecraft attitude estimators [1]. The first considers the case where the angle θ and gyro bias β are estimated from angle and gyro measurements. Dynamic model replacement is used in place of estimating the angular rate ω. The second case has no gyro, and estimates the angle θ and rate ω using the angular sensor and the dynamic model. Markley extended this analysis to the case of a rate-integrating gyro, where the assumed states are θ, β, ω, and the rate-integrated gyro angle ϕ [2]. This analysis assumed that the process noise due to disturbance torques is much larger than all other process and measurement noise variances, and as such the filter ignores the dynamics model and instead employs dynamic model replacement using the rate-integrating gyro. The full three-axis Kalman filter for using rate-integrated gyros is shown in Ref. [3]. Markley also has extended Farrenkopf's steady-state analysis to the three-axis case [4].

All of these dynamic model replacement formulations are sensible when gyro noise is low, as accurate propagation can be carried out from the gyro measurements and bias estimates alone. Micro-Electro-Mechanical System (MEMS) gyros have become increasingly common, specifically in small satellites. The advent of MEMS attitude sensors has enabled precision attitude determination in small satellites. However, MEMS gyros have substantially higher read-noise than conventional gyros. This can lead to poor rate estimates, which can cause poor attitude estimates when used in a dynamic model replacement filter.

An approach that can better handle noisy gyros is to also estimate the angular rate as part of the state vector. In this filter, the attitude θ, angular rate ω, and gyro bias β are estimated. This paper extends a Farrenkopf-type analysis to this formulation, and presents a method to assess when it is appropriate to use this formulation instead of the conventional dynamic model replacement formulation.

Dynamics and Measurement Models

Dynamic Model Replacement

Traditionally, attitude filtering on spacecraft is performed using dynamic model replacement, where the attitude and gyro bias are estimated, and the angular rate estimate is determined by subtracting the bias

*Graduate Student, Department of Mechanical & Aerospace Engineering. Email: andrewdi@buffalo.edu. Student Member AIAA.

†CUBRC Professor in Space Situational Awareness, Department of Mechanical & Aerospace Engineering. Email: johnc@buffalo.edu. Fellow AIAA.

estimate from the gyro reading. A common gyro noise model is [5]

$$\tilde{\omega} = \omega + \beta + \eta_v \tag{1a}$$

$$\dot{\beta} = \eta_u \tag{1b}$$

where $\tilde{\omega}$ is the gyro measurement, β is the bias, and η_v and η_u are zero-mean Gaussian processes with spectral densities σ_v^2 and σ_u^2, respectively. Dynamic model replacement leverages the fact that η_v is very small for most gyroscopes, and the angular rate estimate is determined by estimating the bias vector and subtracting it from the gyro readings:

$$\hat{\omega} = \tilde{\omega} - \hat{\beta} \tag{2}$$

where $\hat{\omega}$ is the angular rate estimate and $\hat{\beta}$ is the bias estimate. This formulation has the advantage that it does not require knowledge of command torques, and does not require process noise compensation for unknown disturbance torques. However, process noise compensation is required in the attitude state to account for the gyro noise, as will be shown.

In the single-axis case, the state vector consists of the angle and gyro bias, denoted by $\boldsymbol{x} = [\theta \quad \beta]^T$. The dynamics of this model are given by

$$\dot{\theta} = \tilde{\omega} - \beta - \eta_v \tag{3}$$

and Eq. (1b). In discrete-time, this model is given by [5]

$$\boldsymbol{x}_{k+1} = \Phi \boldsymbol{x}_k + \Gamma \tilde{\omega}_k + \boldsymbol{w}_k \tag{4}$$

where

$$\Phi = \begin{bmatrix} 1 & -\Delta t \\ 0 & 1 \end{bmatrix} \tag{5a}$$

$$\Gamma = \begin{bmatrix} \Delta t \\ 0 \end{bmatrix} \tag{5b}$$

and Δt is the sampling interval. The covariance of $\boldsymbol{w}_k$ is given by

$$Q = \begin{bmatrix} \sigma_v^2 \Delta t + \frac{1}{3}\sigma_u^2 \Delta t^3 & -\frac{1}{2}\sigma_u^2 \Delta t^2 \\ -\frac{1}{2}\sigma_u^2 \Delta t^2 & \sigma_u^2 \Delta t \end{bmatrix} \tag{6}$$

Note that this process noise covariance contains the gyro noise terms. As the gyro is used directly in the dynamics model, it is not used as a measurement, and as such the measurement vector contains only the attitude (angle) measurement. This means that the angular rate estimate is not filtered to any noise level in the gyro. In fact, as seen from Eq. (3) it is clearly evident that the noise level from the angular rate estimate will be larger than the noise from the gyro measurement due to the noise in the estimated bias. The measurement model is given by

$$\tilde{y}_k = H \boldsymbol{x}_k + v_k \tag{7}$$

where $H = [1 \quad 0]$ and v_k is the noise in the attitude sensor measurement, which is assumed to have variance σ_n^2.

Augmented Filter

Consider a state vector consisting of the angle, angular velocity, and gyro bias, denoted by $\boldsymbol{x} = [\theta \ \ \omega \ \ \beta]^T$. The dynamics of this model are assumed to follow

$$\begin{aligned} \dot{\boldsymbol{x}} &= \begin{bmatrix} 0 & 1 & 0 \\ 0 & 0 & 0 \\ 0 & 0 & 0 \end{bmatrix} \boldsymbol{x} + \begin{bmatrix} 0 & 0 \\ 1 & 0 \\ 0 & 1 \end{bmatrix} \begin{bmatrix} \eta_\omega \\ \eta_u \end{bmatrix} \\ &\equiv F\boldsymbol{x} + G\boldsymbol{w} \end{aligned} \tag{8}$$

where the spectral densities of η_ω and η_u are given by σ_ω^2 and σ_u^2, respectively. Thus, in continuous time, the spectral density of $\boldsymbol{w}$ is

$$Q(t) = \begin{bmatrix} 0 & 0 & 0 \\ 0 & \sigma_\omega^2 & 0 \\ 0 & 0 & \sigma_u^2 \end{bmatrix} \tag{9}$$

The discrete-time model of Eq. (1) is given by

$$\boldsymbol{x}_{k+1} = \Phi \boldsymbol{x} + \boldsymbol{w}_k \tag{10}$$

where

$$\Phi = \begin{bmatrix} 1 & \Delta t & 0 \\ 0 & 1 & 0 \\ 0 & 0 & 1 \end{bmatrix} \tag{11}$$

and the covariance of $\boldsymbol{w}_k$ is given by

$$Q = \begin{bmatrix} \frac{1}{3}\sigma_\omega^2 \Delta t^3 & \frac{1}{2}\sigma_\omega^2 \Delta t^2 & 0 \\ \frac{1}{2}\sigma_\omega^2 \Delta t^2 & \sigma_\omega^2 \Delta t & 0 \\ 0 & 0 & \sigma_u^2 \Delta t \end{bmatrix} \tag{12}$$

From this model it is now possible to filter noisy gyro measurements because the angular rate is modeled as a random walk process in the state vector. At first glance one would expect that as the spectral density of this random walk process increases then the augmented model would approach Farrenkopf's original model because large process noise values tend to place more weight on the measurements, thereby tending to ignore the state model. But, as shown in this paper this intuition does not match reality.

The gyro measurement model is given by

$$\tilde{\omega} = \omega + \beta + \eta_v \tag{13}$$

where the spectral density of η_v is given by σ_v^2. Discrete-time measurements of the angle and angular velocity are assumed, so that the measurement model is given by

$$\begin{aligned} \tilde{\boldsymbol{y}}_k &= \begin{bmatrix} 1 & 0 & 0 \\ 0 & 1 & 1 \end{bmatrix} \boldsymbol{x}_k + \begin{bmatrix} v_{\theta_k} \\ v_{\omega_k} \end{bmatrix} \\ &\equiv H\boldsymbol{x} + \boldsymbol{v}_k \end{aligned} \tag{14}$$

Note that this is no longer a dynamic-model replacement mode setup. This is a more traditional Kalman filter setup where all measurements are embedded in the output vector. The variance of v_{θ_k} is given by σ_n^2. To derive the variance of v_{ω_k}, the following discrete-time gyro and bias model is used [6]:

$$\tilde{\omega}_{k+1} = \omega_{k+1} + \frac{1}{2}\left(\beta_{k+1} + \beta_k\right) + \left(\frac{\sigma_v^2}{\Delta t} + \frac{1}{12}\sigma_u^2 \Delta t\right)^{1/2} N_{v_k} \tag{15a}$$

$$\beta_{k+1} = \beta_k + \sigma_u \Delta t^{1/2} N_{u_k} \tag{15b}$$

where N_{v_k} and N_{u_k} are zero-mean Gaussian white-noise processes with variance each given by one. Substituting Eq. (15b) into Eq. (15a) gives

$$\tilde{\omega}_{k+1} = \omega_{k+1} + \beta_{k+1} - \frac{1}{2}\sigma_u \Delta t^{1/2} N_{u_k} + \left(\frac{\sigma_v^2}{\Delta t} + \frac{1}{12}\sigma_u^2 \Delta t\right)^{1/2} N_{v_k} \tag{16}$$

Since N_{v_k} and N_{u_k} are uncorrelated then the variance of $\tilde{\omega}_{k+1}$ is given by

$$\text{var}\left(\tilde{\omega}_{k+1}\right) = \frac{\sigma_v^2}{\Delta t} + \frac{1}{3}\sigma_u^2 \Delta t \tag{17}$$

Therefore, the covariance of $\boldsymbol{v}_k$ is given by

$$R_k = \begin{bmatrix} \sigma_n^2 & 0 \\ 0 & \frac{\sigma_v^2}{\Delta t} + \frac{1}{3}\sigma_u^2 \Delta t \end{bmatrix} \tag{18}$$

The continuous-time measurement noise covariance $R(t)$ is approximated by [7]

$$R(t) = R_k \Delta t \tag{19}$$

The goal is to determine the steady-state variances for the estimated states given the matrices Φ, H, Q, and R.

Solutions

Farrenkopf's Original Solution

Farrenkopf's original solution is found by setting the pre- and post-update covariances equal for consecutive time steps, i.e.

$$P_k^- = P_{k+1}^- \tag{20a}$$

$$P_k^+ = P_{k+1}^+ \tag{20b}$$

where the superscript "$-$" denotes pre-update and the superscript "$+$" denotes post-update. If the elements of the covariance matrix P_k are denoted as

$$P_k = \begin{bmatrix} \sigma_{\theta\theta}^2 & \sigma_{\theta\beta}^2 \\ \sigma_{\theta\beta}^2 & \sigma_{\beta\beta}^2 \end{bmatrix} \tag{21}$$

then Farrenkopf found the steady-state solutions to be [1]

$$\sigma_{\theta\theta}^- = \sigma_n \sqrt{\left(\frac{x}{S_u}\right)^2 - 1} \tag{22a}$$

$$\sigma_{\theta\theta}^+ = \sigma_n \sqrt{1 - \left(\frac{S_u}{x}\right)^2} \tag{22b}$$

$$\sigma_{\beta\beta}^- = \frac{\sigma_n}{T} \sqrt{S_u^2 \left(\frac{1}{x} + \frac{1}{2}\right) - x} \tag{22c}$$

$$\sigma_{\beta\beta}^+ = \frac{\sigma_n}{T} \sqrt{S_u^2 \left(\frac{1}{x} - \frac{1}{2}\right) - x} \tag{22d}$$

where

$$x = -\frac{1}{2}\left[\left(\frac{S_u^2}{2} + \beta\right) + \sqrt{\left(\frac{S_u^2}{2} + \beta\right)^2 - 4S_u^2}\right] \tag{23a}$$

$$\beta = +\left[S_u^2\left(4 + S_v^2\right) + \frac{S_u^4}{12}\right]^{\frac{1}{2}} \tag{23b}$$

$$S_v = \frac{\sigma_v \left(\Delta t\right)^{\frac{1}{2}}}{\sigma_n} \tag{23c}$$

$$S_u = \frac{\sigma_u \left(\Delta t\right)^{\frac{1}{2}}}{\sigma_n} \tag{23d}$$

The process by which the steady-state covariance elements were solved for was to set each independent element in Eqs. (20a) and (20b), and then substitute the equations until a quartic in $\sigma_{\theta\beta}^2$ is obtained. This quartic was found to be a product of two quadratics, and the appropriate solution is chosen. Then, this can be substituted to solve for $\sigma_{\theta\theta}^2$ and $\sigma_{\beta\beta}^2$.

Augmented Solutions

Setting the pre- and post-update covariances equal in discrete time, as in Farrenkopf's original work and Eq. (20), yields a system of twelve highly coupled nonlinear equations, for which an analytic solution has not been found. However, if the update and propagation steps of the Kalman filter are written as a single step and substituted into Eq. (20a), then

$$P_k^- = \Phi_k P_k^- \Phi_k^T - \Phi_k P_k^- H_k^T \left[H_k P_k^- H_k^T + R_k^{-1}\right]^{-1} H_k P_k^- \Phi_k^T \tag{24}$$

which is a discrete Algebraic Riccati Equation. Solving this equation gives the steady-state pre-update covariance solution. Although a symbolic solution is not found for this case, if the actual noise parameters and time step values that compose P, H, Q, and R are used, the solution value can be found.

The post-update covariance propagation does not take the form of a Riccati equation. However, if the pre-update covariance is found from Eq. (24), the post-update covariance can be found using the standard Kalman Filter update equation:

$$P_k^+ = P_k^- - K_k H P_k^- \tag{25}$$

where the gain K_k is given by

$$K_k = P_k^- H^T [H P_k^- H^T + R]^{-1} \tag{26}$$

This allows the post-update steady-state covariance to be evaluated as well.

The continuous-update limit can be found by setting the covariance rate to zero in the continuous-time filter:

$$\dot{P}(t) = F(t)P(t) + P(t)F^T(t) - P(t)H^T(t)R^{-1}(t)H(t)P(t) + G(t)Q(t)G^T(t) = 0 \tag{27}$$

Both the pre-update and post-update errors approach the continuous-update limit in the limiting case of very frequent updates [6]. Equation (27) is a continuous Algebraic Riccati Equation.

Using the Schur method [8] on the symbolic form of Eq. (27) produces an analytic solution for the continuous time P_k^-. However, this solution is extremely long and is not presented here. As shown in the subsequent section, the continuous time solution is not useful in determining whether to use dynamic model replacement or the augmented filter.

Results

Comparison of Augmented and Dynamic Model Replacement Solutions

The steady-state covariances for the attitude, angular rate, and gyro bias are now computed for many values of σ_ω. Figure 1 shows the absolute difference between the steady-state covariances plotted against σ_ω for the case of an assumed star tracker attitude sensor with $\sigma_n = 2.91 \times 10^{-5}$ rad/s and a mechanical gyro with $\sigma_v = \sqrt{10} \times 10^{-7}$ rad/s and $\sigma_u = \sqrt{10} \times 10^{-10}$ rad/s^2. The sampling time is $\Delta t = 0.01$ s. The absolute difference has been plotted to ensure the result is positive and can be plotted on a log scale. The discrete pre-update (P_k^-), continuous limit, and discrete post-update (P_k^+) values are plotted. The resulting values have been compared to actual filter results to ensure validity.

It is seen that there exists a "sweet spot" for each uncertainty where they are equal, visible in the plots as a sharp dip in the absolute difference. In the presented plots, these dips are not asymptotic due to the finite resolution of σ_ω, but they do represent the zero-crossing. To the left of the "sweet spot", the augmented filter has lower uncertainty and thus better performance, while to the right, the dynamic model replacement filter has lower uncertainty.

Several interesting results are noted. It is seen that for small values of σ_ω, the discrete and continuous-time performance matches almost exactly. However, as σ_ω becomes larger and the sweet spot is approached, the continuous-time solution no longer provides an accurate approximation of the discrete-time performance. The continuous-time solution in fact has its own sweet spot, which is seen to be far past those of the discrete-time solutions. Thus, it is seen that the continuous-time solution does not yield a useful comparison between the two filters, and is not appropriate to use in determining which filter to use.

It is seen that for the attitude estimate, the sweet spot for the pre-update $\sigma_{\theta\theta}^-$ occurs at a lower σ_ω value than the post-update case $\sigma_{\theta\theta}^+$. However, for the bias estimate, it occurs at the same value for both the pre- and post-update cases. The angular rate estimate presents an interesting result, as the difference between the post-update solutions is constant, and the pre-update and continuous solutions have the same sweet

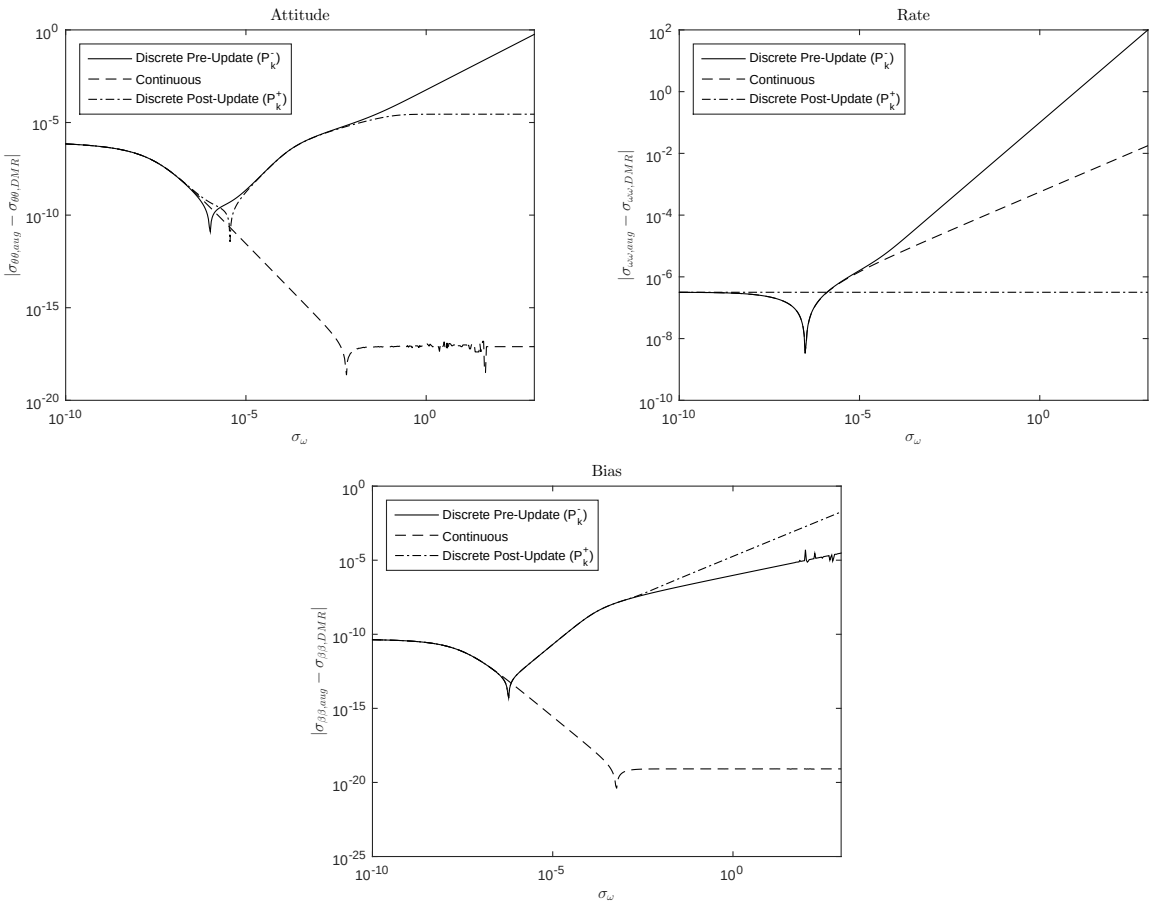

Figure 1. Absolute difference between steady-state covariances of augmented and dynamic model replacement filters for star tracker and mechanical gyros. $\Delta t = 0.01$ **s.**

spot. It is also seen that the sweet spot for the attitude occurs at a larger value of σ_ω than the gyro bias, which in turn occurs at a larger σ_ω than the angular rate. For this case, the pre-update sweet spot occurs at $\sigma_\omega = 1.028 \times 10^{-6}$ rad/s^2 for the attitude, $\sigma_\omega = 5.992 \times 10^{-7}$ for the bias, and $\sigma_\omega = 3.097 \times 10^{-7}$ for the rate.

The same analysis is now run again with the assumption that the gyros have been replaced with MEMS gyros, which have substantially higher noise properties. In this case, it is assumed that $\sigma_v = 3.473 \times 10^{-4}$ rad/s, $\sigma_u = 1.309 \times 10^{-4}$ rad/s^2, and σ_n remains unchanged at 2.91×10^{-5}. The results of this case are shown in Fig. 2.

It is seen that in this case, all of the sweet spots have shifted to the right, or to a greater value of σ_ω. The attitude sweet spot is increased to $\sigma_\omega = 3.112 \times 10^{-2}$, a substantial increase from the value of $\sigma_\omega = 1.028 \times 10^{-6}$ for the mechanical gyro case. This indicates that the augmented state choice should be employed for higher values of σ_ω in the MEMS gyro case than in the mechanical gyro case. This is intuitive, as dynamic model replacement uses the gyro reading directly for determining the rate estimate and thus for propagating the attitude, as opposed to estimating the rate in the filter. The higher noise in the gyro readings means that there is more uncertainty in the rate estimate, which leads to more uncertainty in the propagated attitude estimate.

Other than the shifting of the sweet spots to the right, this case experiences the similar behaviors as the previous case. The pre-update attitude sweet spot still occurs at a slightly smaller σ_ω than the post-update value. The sweet spots in the continuous-time solution occur at a much greater σ_ω than the pre-update discrete solution for the attitude and bias estimates, and the continuous-time solution is again seen to be a poor choice for determining which filter model to use. The pre-update sweet spot for attitude occurs at a larger σ_ω than for the gyro bias, which occurs at a larger σ_ω than for the angular rate. Here, the sweet spot

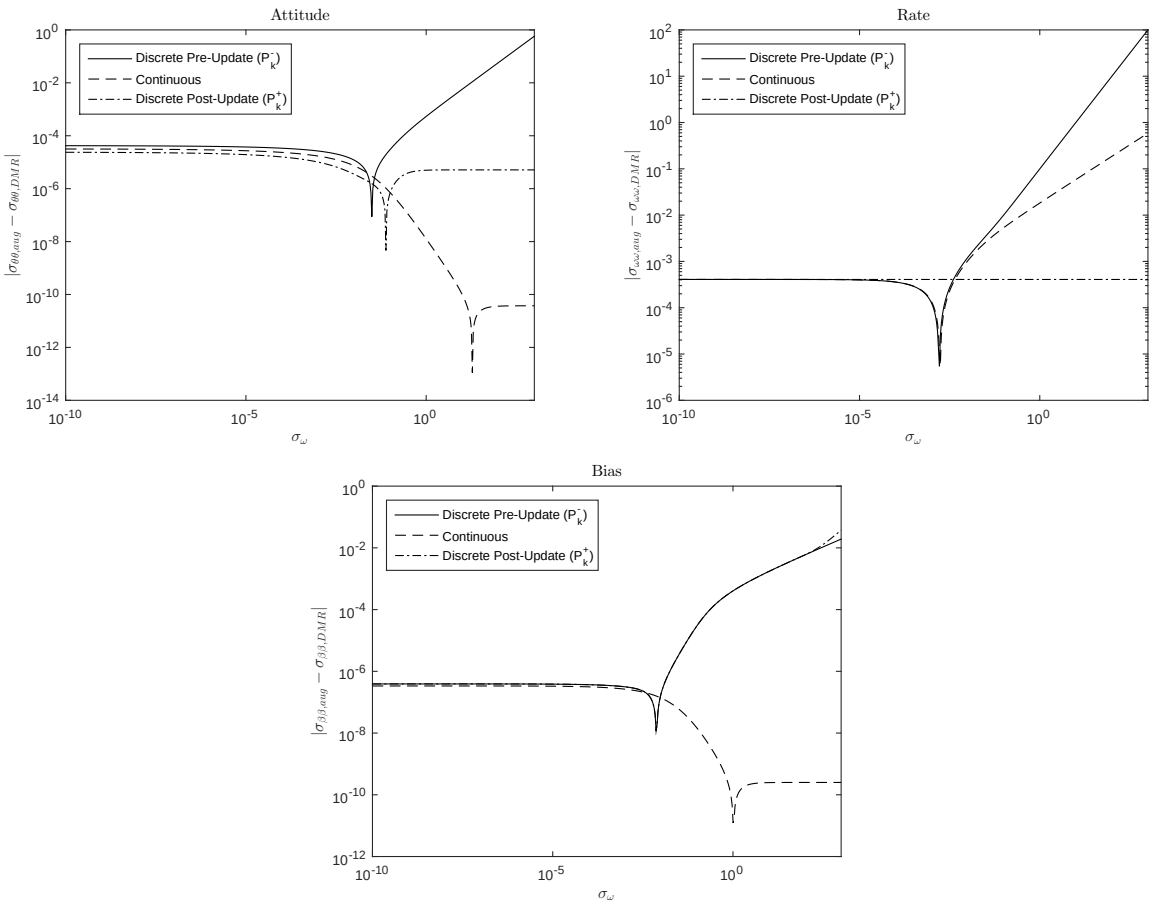

Figure 2. Absolute difference between steady-state covariances of augmented and dynamic model replacement filters for star tracker and MEMS gyros, $\Delta t = 0.01$ s.

for the attitude occurs at $\sigma_\omega = 3.112 \times 10^{-}2$ rad/s^2, for the gyro bias occurs at $\sigma_\omega = 7.375 \times 10^{-3}$ rad/s^2, and for the angular rate occurs at $\sigma_\omega = 1.748 \times 10^{-3}$ rad/s^2.

Figure 3 plots the value of σ_ω corresponding to the sweet spot against σ_v. Although both σ_v and σ_u contribute to the steady-state solutions, the effect of σ_v in the dynamic model replacement case dominates σ_u. This can be seen by examining the upper-left term of Q ($\sigma_v^2 \Delta t + 1/3\sigma_u^2 \Delta t^3$) for $\Delta t < 1$. It is evident that as σ_v increases, the value of the sweet spot, where the filter performance in $\sigma_{\theta\theta}$ is equivalent, increases. In this plot, if given σ_v and σ_v values fall below this line, the augmented filter will have better performance. Above this line, dynamic model replacement will perform better.

Impact of Changing Sampling Interval

Now, the impact of changing the sampling interval Δt on the location of the sweet spot is analyzed. Note that the impact of Δt on the actual filtering performance itself is not presented, rather the impact of Δt on the difference between the augmented and dynamic model replacement filters is presented. The first case, with assumed mechanical gyros with $\sigma_v = \sqrt{10} \times 10^{-7}$ rad/s and $\sigma_u = \sqrt{10} \times 10^{-10}$ rad/s^2 is simulated, but this time with Δt decreased to 0.001 s. The results of this case are presented in Fig. 4. All of the sweet spots shift to the right, to a higher σ_ω. The pre-update attitude sweet spot is found to be $\sigma_\omega = 5.514 \times 10^{-6}$ rad/s^2, the bias sweet spot $\sigma_\omega = 2.528 \times 10^{-6}$ rad/s^2, and the rate sweet spot $\sigma_\omega = 3.289 \times 10^{-7}$ rad/s^2. This shift toward higher values of σ_ω is explained by the lessened effect of the same σ_ω over a shorter time period Δt in the augmented filter. As Δt becomes smaller, the augmented filter is better able to handle increased values of σ_ω. However, the impact of reducing Δt becomes smaller is Δt itself becomes smaller, and decreasing Δt is not as effective as shifting the σ_ω sweet spot to the right as improving the sensor noise characteristics. Figure 5 shows the value of σ_ω corresponding to the sweet spot, where the filter performance

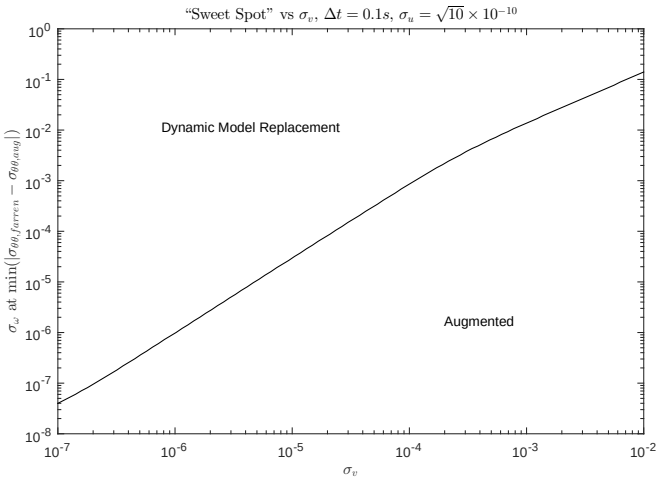

Figure 3. "Sweet Spot" σ_ω value vs σ_v

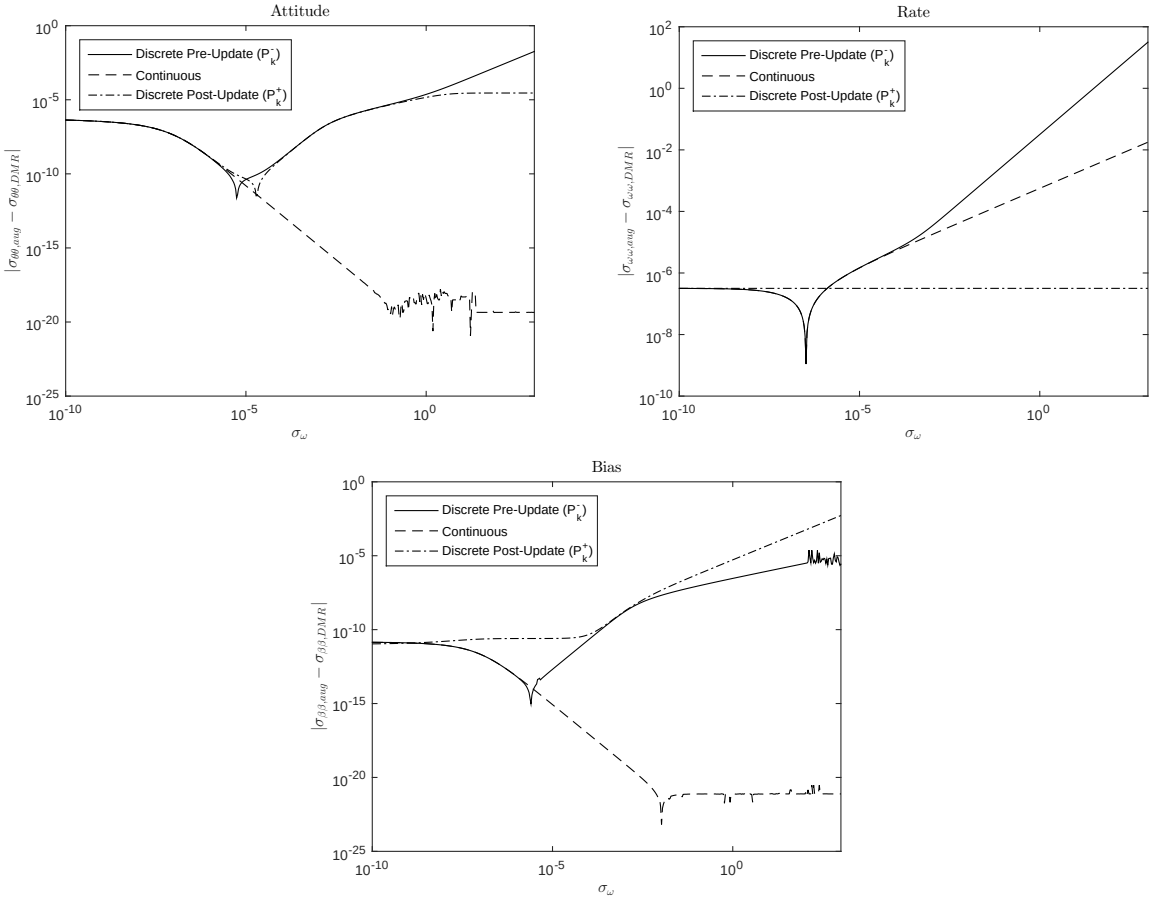

Figure 4. Absolute difference between steady-state covariances of augmented and dynamic model replacement filters for star tracker and mechanical gyros, $\Delta t = 0.001$ s.

in $\sigma_{\theta\theta}$ is equal for both models, as Δt is varied. The diminishing effect of varying Δt on the sweet spot is evident.

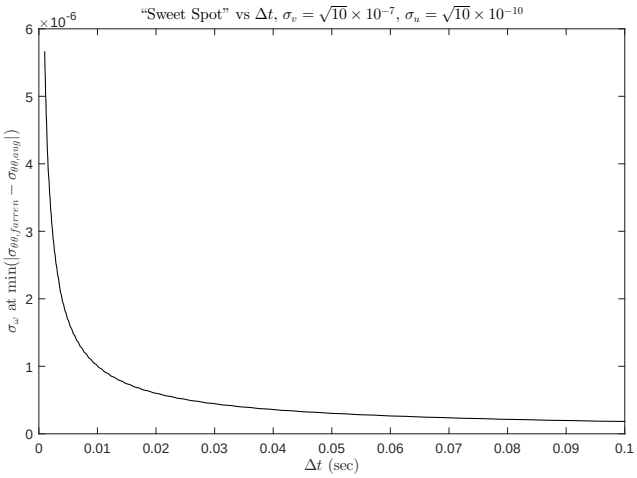

Figure 5. "Sweet Spot" σ_ω value vs Δt

Impact of Modeling Errors

The previous sections provide considerations for choosing between the augmented and dynamic model replacement filters assuming that σ_ω is known, and is zero-mean Gaussian. However, in real applications, σ_ω is often not well-known. If the real σ_ω is larger than assumed in the filter, or has a bias, the true filter error will not remain bounded by the 3σ bounds, and the true error will not approach the calculated steady-state value. Conversely, if the real σ_ω is smaller than assumed, the true filter error will be much smaller than the 3σ bounds, and the true error will be smaller than the calculated steady-state value. While this does not present the danger of filter divergence, it results in a filter that does not perform as well as one that is well-tuned. Figure 6 shows the performance of augmented filters with σ_ω assumed too small and too large.

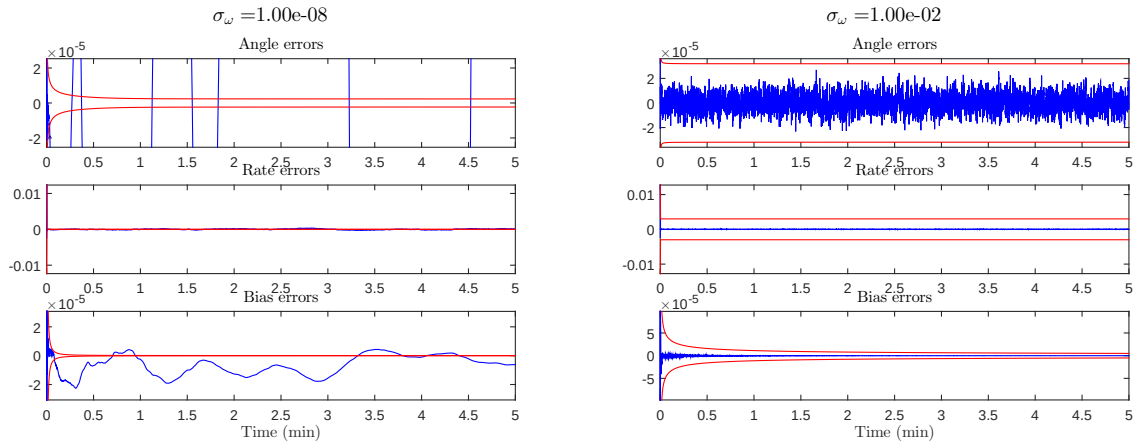

Figure 6. Filter results with σ_ω assumed too small (left) and too large (right). Actual $\sigma_\omega = 3.33 \times 10^{-5}$.

Multiple Model Adaptive Estimation

One method that can improve performance if σ_ω is not well-known is to use Multiple-Model Adaptive Estimation (MMAE). In MMAE, a bank of filters are run in parallel, in this case, with a different assumed σ_ω in each filter. A derivation of the MMAE process can be found in [7]. Given the j^{th} probability density function $p(\tilde{\boldsymbol{y}}_k|\hat{\boldsymbol{x}}_k^{-(j)})$, the MMAE weights are computed as

$$w_k^{(j)} = w_{k-1}^{(j)} p(\tilde{\boldsymbol{y}}_k|\hat{\boldsymbol{x}}_k^{-(j)}) \tag{28}$$

which then must be normalized by

$$w_k^{(j)} \leftarrow \frac{w_k^{(j)}}{\sum_{j=1}^{M} w_k^{(j)}} \tag{29}$$

where $\leftarrow$ denotes replacement, and M is the total number of filters used. Also, the weights give the probability of the j^{th} filter's contribution. Assuming the measurement model is Gaussian, the probability density function $p(\tilde{\boldsymbol{y}}_k|\hat{\boldsymbol{x}}_k^{-(j)})$ is given by

$$p(\tilde{\boldsymbol{y}}_k|\hat{\boldsymbol{x}}_k^{-(j)} = \frac{1}{[\det(2\pi E_k^{-(j)})]^{1/2}} \exp\left\{-\frac{1}{2}\boldsymbol{e}_k^{-(j)T}(E_k^{-(j)})^{-1}\boldsymbol{e}_k^{-(j)}\right\} \tag{30}$$

where

$$\boldsymbol{e}_k^{-(j)} \equiv \tilde{\boldsymbol{y}}_k - \hat{\boldsymbol{y}}_k^{-(j)} \tag{31}$$

and

$$E_k^{-(j)} \equiv H_k^{(j)} P_k^{-(j)} H_k^{(j)T} + R_k^{(j)} \tag{32}$$

The truth case is simulated with an assumed $\sigma_\omega = 3.33 \times 10^{-5}$ rad/s^2. MMAE is run with a bank of 80 filters logarithmically spaced between 10^{-6} and 10^{-2}. Figure 7 shows the MMAE weights and the filter performance. MMAE drives the weight of the filter with $\sigma_\omega = 3.3036 \times 10^{-5}$ to one. This is the closest σ_ω value to the truth. The filter is seen to be well-tuned.

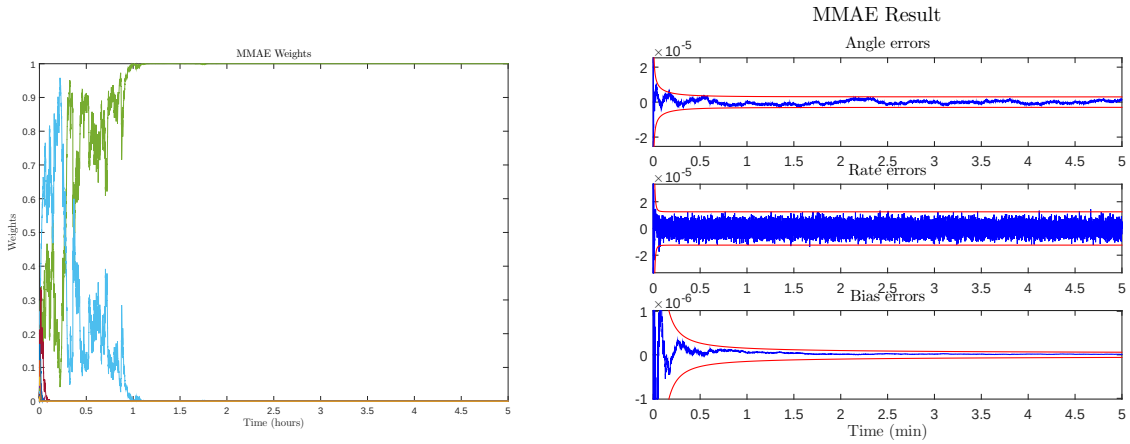

Figure 7. MMAE weights (left) and MMAE filter performance (right). Filter weight that goes to one (depicted in green) corresponds to $\sigma_\omega = 3.3036 \times 10^{-5}$.

Comparison to Three-Axis Case

The above analysis has been performed for a single-axis case. Practical applications will involve three-axis attitude determination. Markley [4] has extended Farrenkopf's steady state analysis to the three-axis case, but this does not consider the augmented case where the angular rate is estimated as a filter state. As seen in the single-axis case, augmenting the filter states with the angular rate increases the complexity of the filter propagation and update equations drastically, and as such it is unlikely that an analytic solution exists. This section will compare three-axis filtering results to single-axis results to assess whether a single-axis analysis is appropriate to consider in the design of a three-axis system.

Quaternion Kinematics

First, an overview of the three-axis attitude dynamics is given. Although a spacecraft's attitude is described by three degrees of freedom, there exist no nonsingular three parameter representations. The quaternion, a four-parameter realization, is one of the most commonly used representations in attitude determination. It

is composed of a 3×1 vector ϱ and a scalar q_4:

$$\boldsymbol{q} = \begin{bmatrix} \boldsymbol{\varrho}^T & q_4 \end{bmatrix}^T \tag{33}$$

The quaternion is subject to the constraint $||\boldsymbol{q}|| = 1$. Unless otherwise noted, the quaternion describes the rotation from the inertial frame to the spacecraft body frame.

The spacecraft's angular rate, measured with respect to an inertial frame but written in body-frame coordinates, is denoted $\boldsymbol{\omega}$, a 3×1 vector. Then, the quaternion kinematics are given by [6]

$$\dot{\boldsymbol{q}} = \frac{1}{2}\Xi(\boldsymbol{q})\boldsymbol{\omega} = \frac{1}{2}\Omega(\boldsymbol{\omega})\boldsymbol{q} \tag{34}$$

where

$$\Xi(\boldsymbol{q}) = \begin{bmatrix} q_4 I_{3\times 3} + [\boldsymbol{\varrho}\times] \\ -\boldsymbol{\varrho}^T \end{bmatrix} \tag{35a}$$

$$\Omega(\boldsymbol{\omega}) = \begin{bmatrix} -[\boldsymbol{\omega}\times] & \boldsymbol{\omega} \\ -\boldsymbol{\omega}^T & 0 \end{bmatrix} \tag{35b}$$

where $I_{3\times 3}$ is the 3×3 identity matrix and $[\boldsymbol{\omega}\times]$ denotes the skew-symmetric cross product matrix of $\boldsymbol{\omega}$.

Kalman Filter Attitude State Formulations

Due to the unit norm constraint, the quaternion cannot be used directly in the Kalman filter, as the constraint may be violated. A common approach to using the quaternion in the Extended Kalman Filter and Multiplicative Extended Kalman Filter (MEKF), which maintains the unit norm to first order. Derivations of the and MEKF are widely available [7, 9]. The MEKF is widely used due to its simplicity. In the MEKF, the true attitude is written as a product of the estimated attitude and a deviation from the estimate. If the error quaternion is defined as $\boldsymbol{\delta q}$, then the true quaternion is written as

$$\boldsymbol{q} = \boldsymbol{\delta q} \otimes \hat{\boldsymbol{q}} \tag{36}$$

Note that quaternion multiplication $\otimes$ is defined using the Shuster convention, where quaternions are composed in the same order as attitude matrices [10]. Here, the error quaternion $\boldsymbol{\delta q}$ is the deviation from the estimate. It can be written as

$$\boldsymbol{\delta q} = \begin{bmatrix} \boldsymbol{\delta\varrho}^T & \delta q_4 \end{bmatrix}^T \tag{37}$$

The attitude states used in the filter are $\boldsymbol{\delta\varrho}$, and the scalar part of the error quaternion is computed as

$$\delta q_4 = \sqrt{1 - ||\boldsymbol{\delta\varrho}||} \tag{38}$$

In the MEKF, the estimated attitude states are $\boldsymbol{\delta\varrho}$. At each time step k, the error quaternion $\boldsymbol{\delta q}$ is initialized as identity:

$$\boldsymbol{\delta q}_k^- = \begin{bmatrix} 0 & 0 & 0 & 1 \end{bmatrix}^T \tag{39}$$

Then, the Kalman update is performed on $\boldsymbol{\delta\varrho}$ and the updated error quaternion is written as

$$\boldsymbol{\delta q}_k^+ = \begin{bmatrix} (\boldsymbol{\delta\varrho}_k^+)^T & \delta q_{4,k}^+ \end{bmatrix}^T \tag{40}$$

where $\delta q_{4,k}^+$ is computed using Eq. (38). Then, the updated quaternion estimate at each time step is given by applying Eq. (36)

$$\hat{\boldsymbol{q}}_k^+ = \boldsymbol{\delta q}_k^+ \otimes \hat{\boldsymbol{q}}_k^- \tag{41}$$

Alternatively, if $\boldsymbol{\delta\varrho}$ is small, then a first-order approximation can be made [6]

$$\hat{\boldsymbol{q}}_k^+ \approx \left(\boldsymbol{I}_q + \begin{bmatrix} \boldsymbol{\delta\varrho}_k^+ \\ 0 \end{bmatrix} \right) \otimes \hat{\boldsymbol{q}}_k^- = \hat{\boldsymbol{q}}_k^- + \boldsymbol{\delta\varrho}_k^+ \otimes \hat{\boldsymbol{q}}_k^- = \hat{\boldsymbol{q}}_k^- + \Xi(\hat{\boldsymbol{q}})\boldsymbol{\delta\varrho} \tag{42}$$

where $\boldsymbol{I}_q$ is the identity quaternion. In this approach, the quaternion must be re-normalized after every update step. With the attitude parameterizations of the MEKF now defined, forms of the MEKF will be presented for both the cases of dynamic model replacement and a full-state filter including angular rate.

Dynamic Model Replacement Filter

Dynamic Model Replacement is carried out in the same manner as the single-axis case. Equation (8) is written in vector form as

$$\tilde{\boldsymbol{\omega}} = \boldsymbol{\omega} + \boldsymbol{\beta} + \boldsymbol{\eta}_v \tag{43a}$$

$$\dot{\boldsymbol{\beta}} = \boldsymbol{\eta}_u \tag{43b}$$

where $\tilde{\boldsymbol{\omega}}$ is the three-axis gyro measurement, $\boldsymbol{\beta}$ is the bias vector, and $\boldsymbol{\eta}_v$ and $\boldsymbol{\eta}_u$ are zero-mean Gaussian processes with spectral densities $\sigma_v^2 I_{3\times3}$ and $\sigma_u^2 I_{3\times3}$, respectively. Equation (2) is written in vector form as

$$\hat{\boldsymbol{\omega}} = \tilde{\boldsymbol{\omega}} - \hat{\boldsymbol{\beta}} \tag{44}$$

where $\hat{\boldsymbol{\omega}}$ is the angular rate vector estimate and $\hat{\boldsymbol{\beta}}$ is the bias vector estimate.

The estimated states in the filter are the attitude and the bias vector. A full derivation of this filter can be found in [6], and only its key components are summarized here for brevity. The attitude is represented using the form of the MEKF presented earlier, except the attitude state is represented as $\boldsymbol{\delta\alpha}$, where

$$\boldsymbol{\delta\alpha} = 2\boldsymbol{\delta\varrho} \tag{45}$$

This formulation is chosen as it simplifies the attitude kinematics. Additionally, $\boldsymbol{\delta\alpha}$ has physical significance as errors in roll, pitch, and yaw. Defining the error in the angular rate and bias estimates to be

$$\boldsymbol{\delta\omega} \equiv \boldsymbol{\omega} - \hat{\boldsymbol{\omega}} \tag{46a}$$

$$\boldsymbol{\Delta\beta} \equiv \boldsymbol{\beta} - \hat{\boldsymbol{\beta}} \tag{46b}$$

and substituting Equations (43a) and (44) yields

$$\boldsymbol{\delta\omega} = -(\boldsymbol{\Delta\beta} + \boldsymbol{\eta}_v) \tag{47}$$

Substituting Equations (45) and (47) into the quaternion kinematics given in Eq. (34) gives the linearized error-state kinematics:

$$\boldsymbol{\delta\dot{\alpha}} = -[\boldsymbol{\omega}\times]\boldsymbol{\delta\alpha} - (\boldsymbol{\Delta\beta} + \boldsymbol{\eta}_v) \tag{48}$$

The EKF state vector is given by

$$\boldsymbol{\Delta x}(t) = \begin{bmatrix}\boldsymbol{\delta\alpha}(t)^T & \boldsymbol{\Delta\beta}(t)^T\end{bmatrix}^T \tag{49}$$

and the linearized error model is given by

$$\boldsymbol{\Delta\dot{x}}(t) = F(t)\boldsymbol{x}(t) + G(t)\boldsymbol{w}(t) \tag{50}$$

where

$$\boldsymbol{w}(t) = \begin{bmatrix}\boldsymbol{\eta}_v(t)^T & \boldsymbol{\eta}_u(t)^T\end{bmatrix}^T \tag{51}$$

and

$$F(t) = \begin{bmatrix}-[\hat{\boldsymbol{\omega}}(t)\times] & -I_{3\times3} \\ 0_{3\times3} & 0_{3\times3}\end{bmatrix} \tag{52a}$$

$$G(t) = \begin{bmatrix}-I_{3\times3} & 0_{3\times3} \\ 0_{3\times3} & I_{3\times3}\end{bmatrix} \tag{52b}$$

Since the gyro readings appear directly in the measurement model, the gyro noise $\boldsymbol{\eta}_v$ appears as process noise in the attitude state. The process noise spectral density matrix is written as

$$Q(t) = \begin{bmatrix}\sigma_v^2 I_{3\times3} & 0_{3\times3} \\ 0_{3\times3} & \sigma_u^2 I_{3\times3}\end{bmatrix} \tag{53}$$

In discrete-time, the state transition matrix is [5]

$$\Phi = \begin{bmatrix}\Phi_{11} & \Phi_{12} \\ \Phi_{21} & \Phi_{22}\end{bmatrix} \tag{54a}$$

$$\Phi_{11} = I_{3\times3} - [\hat{\boldsymbol{\omega}}\times]\frac{\sin(||\hat{\boldsymbol{\omega}}||\Delta t)}{||\hat{\boldsymbol{\omega}}} + [\hat{\boldsymbol{\omega}}\times]^2\frac{1-\cos(||\hat{\boldsymbol{\omega}}||\Delta t)}{||\hat{\boldsymbol{\omega}}||^2} \tag{54b}$$

$$\Phi_{12} = [\hat{\boldsymbol{\omega}}\times]\frac{1-\cos(||\hat{\boldsymbol{\omega}}||\Delta t)}{||\hat{\boldsymbol{\omega}}||^2} - I_{3\times3}\Delta t - [\hat{\boldsymbol{\omega}}\times]^2\frac{||\hat{\boldsymbol{\omega}}||\Delta t - \sin(||\hat{\boldsymbol{\omega}}||\Delta t)}{||\hat{\boldsymbol{\omega}}||^3} \tag{54c}$$

$$\Phi_{21} = 0_{3\times3} \tag{54d}$$

$$\Phi_{22} = I_{3\times3} \tag{54e}$$

The process noise covariance matrix is analogous to that of Eq. (6):

$$Q = \begin{bmatrix} \left(\sigma_v^2\Delta t + \frac{1}{3}\sigma_u^2\Delta t^3\right) I_{3\times3} & \left(\frac{1}{2}\sigma_u^2\Delta t^2\right) I_{3\times3} \\ \left(\frac{1}{2}\sigma_u^2\Delta t^2\right) I_{3\times3} & \left(\sigma_u^2\Delta t\right) I_{3\times3} \end{bmatrix} \tag{55}$$

Attitude measurements are typically unit vector measurements, for example from a star tracker, sun sensor, magnetometer, or earth horizon sensor. If these measurements are denoted $\tilde{\boldsymbol{b}}_1$, $\tilde{\boldsymbol{b}}_2$, ..., $\tilde{\boldsymbol{b}}_n$, the measurement vector at time k is then given by

$$\tilde{\boldsymbol{y}}_k = \begin{bmatrix} \tilde{\boldsymbol{b}}_{1,k}^T & \tilde{\boldsymbol{b}}_{2,k}^T & \dots & \tilde{\boldsymbol{b}}_{n,k}^T \end{bmatrix}^T \tag{56}$$

and the measurements can be modeled as

$$\tilde{\boldsymbol{y}}_k = \begin{bmatrix} (A(\boldsymbol{q})\boldsymbol{r}_1)^T & (A(\boldsymbol{q})\boldsymbol{r}_2)^T & \dots & (A(\boldsymbol{q})\boldsymbol{r}_n)^T \end{bmatrix}^T + \boldsymbol{v}_k \tag{57}$$

where v_k is the measurement noise. The vector measurements are unit vectors, and thus the 3×3 covariance matrix R would be singular. However, Shuster has shown that for the MEKF, this can be replaced with [11]

$$R_k = \text{diag}\begin{bmatrix} \sigma_1^2 I_{3\times3} & \sigma_2^2 I_{3\times3} & \dots & \sigma_n^2 I_{3\times3} \end{bmatrix} \tag{58}$$

The sensitivity matrix for all the measurements is given by

$$H_k(\hat{\boldsymbol{x}}_k^-) = \begin{bmatrix} [A(\hat{\boldsymbol{q}}^-)\boldsymbol{r}_1\times] & 0_{3\times3} \\ [A(\hat{\boldsymbol{q}}^-)\boldsymbol{r}_2\times] & 0_{3\times3} \\ \vdots & \vdots \\ [A(\hat{\boldsymbol{q}}^-)\boldsymbol{r}_n\times] & 0_{3\times3} \end{bmatrix} \tag{59}$$

The standard EKF update and covariance propagation can now be applied.

Augmented Filter

The augmented filter uses a similar MEKF formulation to the dynamic model replacement version, except now there are 9 estimated states instead of 6. The state vector now contains the angular velocity vector:

$$\hat{\boldsymbol{x}} = \begin{bmatrix} \boldsymbol{\delta\alpha}^T & \hat{\boldsymbol{\omega}}^T & \hat{\boldsymbol{\beta}}^T \end{bmatrix}^T \tag{60}$$

The state transition matrix is given by

$$\Phi = \begin{bmatrix} \Phi_{11} & \Phi_{12} & 0_{3\times3} \\ 0_{3\times3} & I_{3\times3} & 0_{3\times3} \\ 0_{3\times3} & 0_{3\times3} & I_{3\times3} \end{bmatrix} \tag{61}$$

where Φ_{11} and Φ_{12} are the same as in Eq. (54). The process noise covariance is analogous to the single-axis case of Eq. (12):

$$Q = \begin{bmatrix} \frac{1}{3}\sigma_\omega^2\Delta t^3 I_{3\times3} & \frac{1}{2}\sigma_\omega^2\Delta t^2 I_{3\times3} & 0_{3\times3} \\ \frac{1}{2}\sigma_\omega^2\Delta t^2 I_{3\times3} & \sigma_\omega^2\Delta t I_{3\times3} & 0_{3\times3} \\ 0_{3\times3} & 0_{3\times3} & \sigma_u^2\Delta t I_{3\times3} \end{bmatrix} \tag{62}$$

The measurement vector now includes the gyro measurements as well as the vector attitude measurements:

$$\tilde{\boldsymbol{y}}_k = \begin{bmatrix} \tilde{\boldsymbol{b}}_{1,k}^T & \tilde{\boldsymbol{b}}_{2,k}^T & \dots & \tilde{\boldsymbol{b}}_{n,k}^T & \tilde{\boldsymbol{\omega}}_k^T \end{bmatrix}^T \tag{63}$$

Referring to the gyro measurement model in Eq. (43a), the measurement sensitivity matrix is

$$H_k(\hat{\boldsymbol{x}}_k^-) = \begin{bmatrix} [A(\hat{\boldsymbol{q}}^-)\boldsymbol{r}_1\times] & 0_{3\times3} & 0_{3\times3} \\ [A(\hat{\boldsymbol{q}}^-)\boldsymbol{r}_2\times] & 0_{3\times3} & 0_{3\times3} \\ \vdots & \vdots & \vdots \\ [A(\hat{\boldsymbol{q}}^-)\boldsymbol{r}_n\times] & 0_{3\times3} & 0_{3\times3} \\ 0_{3\times3} & I_{3\times3} & I_{3\times3} \end{bmatrix} \tag{64}$$

The standard EKF update and propagation steps are now applied.

Results

The three-axis filter is run for both the augmented and dynamic model replacement filters for the first case of a mechanical gyro ($\sigma_v = \sqrt{10}\times10^{-7}$, $\sigma_u = \sqrt{10}\times10^{-10}$) and star tracker ($\sigma_n = 2.91\times10^{-5}$), but with an update interval of $\Delta t = 1$ s. A value of $\sigma_\omega = 5\times10^{-5}$ rad/s^2 is assumed. Here, the star tracker is simulated using an actual star catalog, with noise added to the measurement of each star. Figure 8 shows the attitude, angular velocity, and bias estimate errors for this case of the augmented filter. The results of the augmented filter and a comparison to the single-axis steady-state solution are presented in Table 1. It is seen that for

Table 1. Three-Axis Augmented Filter Steady-State Results

Quantity	Single-Axis Pre-Update	Axis 1 Filter	Axis 2 Filter	Axis 3 filter
Attitude	3.409×10^{-5} rad	3.711×10^{-5} rad	4.073×10^{-5} rad	6.589×10^{-5} rad
Angular Rate	5.000×10^{-5} rad/s	5.000×10^{-5} rad/s	5.000×10^{-5} rad/s	5.000×10^{-5} rad/s
Gyro Bias	6.757×10^{-8} rad/s	6.827×10^{-8} rad/s	6.830×10^{-8} rad/s	2.080×10^{-7} rad/s

two of the axes, the attitude solutions are very close to the expected single-axis value. The third axis is the axis along the star tracker boresight, which explains the greater inaccuracy in this axis. It is found that across all three axes, the angular rate results match exactly to the single-axis value. From these results, it is reasonable to conclude that the single-axis case makes a reasonably good approximation of the three-axis case, notably in the directions perpendicular to the star tracker boresight.

Conclusion

A method by which to evaluate the expected steady-state covariance for the augmented and dynamic model replacement attitude estimators has been presented. If the pre-update covariance is to be analyzed, the steady-state solution can be determined from the solution to a Riccati equation. It is found that the "sweet spot" in σ_ω, at which the augmented filter performs better for smaller values of σ_ω, is different depending on whether attitude, angular rate, or bias is considered, and that for all cases that have been simulated, the attitude sweet spot occurs at the highest σ_ω. As knowledge of the attitude itself is typically the most desired quantity, this value may be of interest in initial filter design. It is shown that decreasing the time step pushes this point toward a larger σ_ω, but that this impact is lessened as σ_ω becomes increasingly small. The impact of incorrect assumptions about σ_ω has been presented and it is seen that incorrectly assuming σ_ω can cause poor filter performance in the augmented filter. Multiple-Model Adaptive Estimation has been found to be a method to overcome this, and is demonstrated to give better filter performance. The three-axis case is simulated and the steady-state covariance is found to be similar to that of the single-axis case, which suggests that using a single-axis steady-state analysis when selecting the choice of filter states could be beneficial.

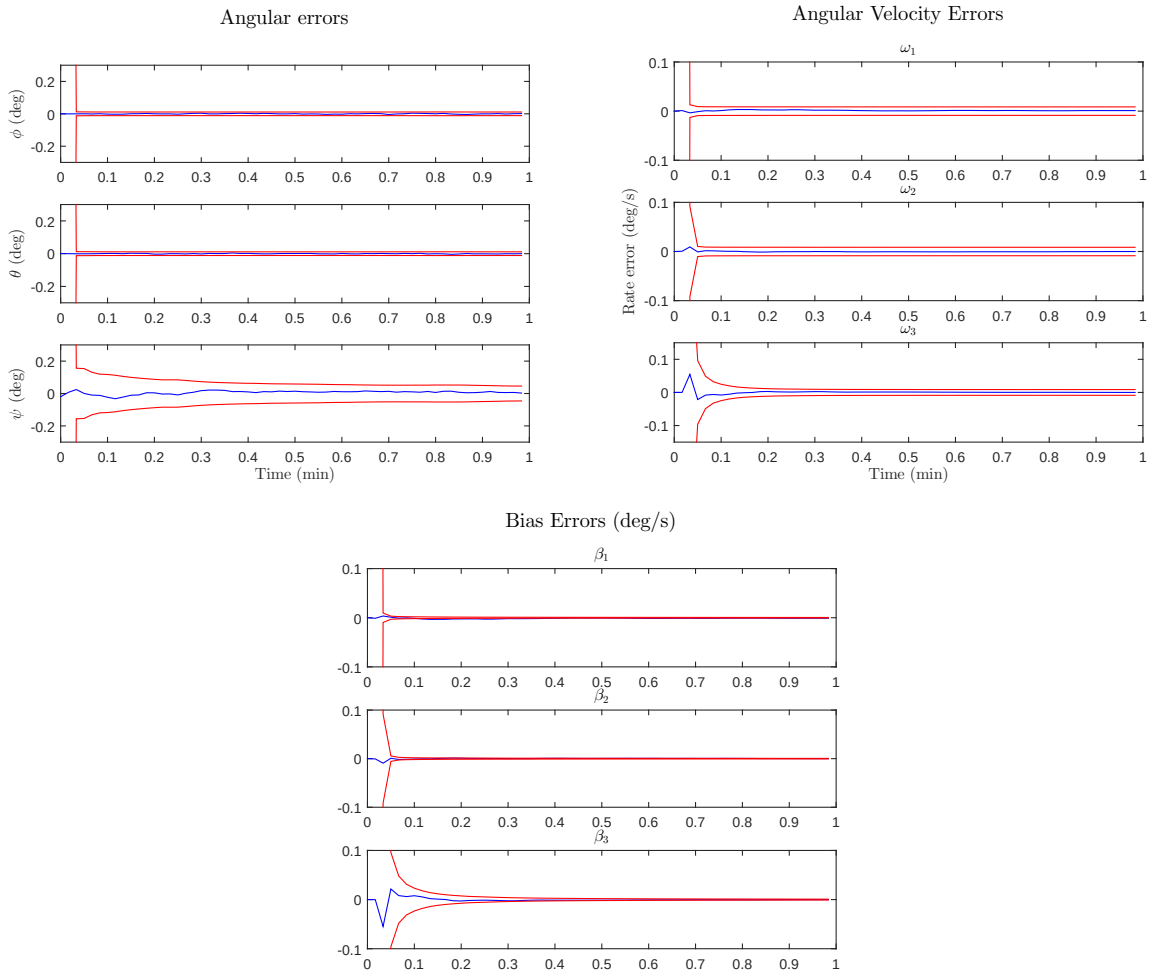

Figure 8. Augmented 3-axis Filter Errors

References

[1]Farrenkopf, R., "Analytic Steady-State Accuracy Solutions for Two Common Spacecraft Attitude Estimators," *Journal of Guidance and Control*, Vol. 1, No. 4, July-Aug. 1978, pp. 282–284.

[2]Markley, F. and Reynolds, R., "Analytic Steady-State Accuracy of a Spacecraft Attitude Estimator," *Journal of Guidance, Control, and Dynamics*, Vol. 23, No. 6, Nov.-Dec. 2000, pp. 1065–1067, doi:10.2514/2.4648.

[3]Crassidis, J. and Markley, F., "Three-Axis Attitude Estimation Using Rate-Integrating Gyroscopes," *Journal of Guidance, Control, and Dynamics*, Vol. 39, No. 7, July 2016, pp. 1513–1526, doi:10.2514/1.G000336.

[4]Markley, F., "Analytic Steady-State Accuracy of a Three-Axis Spacecraft Attitude Estimator," *Journal of Guidance, Control, and Dynamics*, Vol. 40, No. 9, Sept. 2017, pp. 2399–2400, doi:10.2514/1.G000641.

[5]Crassidis, J. and Junkins, J., *Optimal Estimation of Dynamic Systems*, chap. 4, Chapman & Hall/CRC, Boca Raton, FL, 2nd ed., 2012.

[6]Markley, F. and Crassidis, J., *Fundamentals of Spacecraft Attitude Dynamics and Control*, Springer, 2014.

[7]Crassidis, J., Markley, F., and Cheng, Y., "Survey of Nonlinear Attitude Estimation Methods," *Journal of Guidance, Control, and Dynamics*, Vol. 30, No. 1, Jan.-Feb. 2007, pp. 12–28, doi:10.2514/1.22452.

[8]Laub, A., "A Schur Method for Solving Algebraic Riccati Equations," *1978 IEEE Conference on Decision and Control*, IEEE, January 1978.

[9]Markley, F., "Multiplicative vs. Additive Filtering for Spacecraft Attitude Determination," *6th Cranfield Conference on Dynamics and Control of Systems and Structures in Space*, edited by S. Hobbs, Cranfield University Press, Cranfield, Bedford, UK, 2004, pp. 467–474.

[10]Lefferts, E., Markley, F., and Shuster, M., "Kalman Filtering for Spacecraft Attitude Estimation," *Journal of Guidance, Control, and Dynamics*, Vol. 5, No. 5, 1982, pp. 417–429.

[11]Shuster, M., "Maximum Likelihood Estimation of Spacecraft Attitude," *The Journal of the Astronautical Sciences*, Vol. 37, No. 1, Jan.-March 1989, pp. 79–88.